IEEE Access
Multidisciplinary | Rapid Review | Open Access Journal

Received December 24, 2020, accepted January 11, 2021, date of publication January 18, 2021, date of current version January 26, 2021.

*Digital Object Identifier 10.1109/ACCESS.2021.3051949*

# Phase Progression of a Radiation Field From Circular and Square Active Regions

**HISAMATSU NAKANO, (Life Fellow, IEEE), TOMOKI ABE, (Member, IEEE), AND JUNJI YAMAUCHI, (Life Fellow, IEEE)**
Department of Science and Engineering, Hosei University, Tokyo 184-8584, Japan

Corresponding author: Hisamatsu Nakano (hymat@hosei.ac.jp)

This work was supported in part by the Japan Society for the Promotion of Science (JSPS) KAKENHI under Grant JP18K04154.

**ABSTRACT** The radiation generated by the current in an active region (ACT-R), specified by propagation phase constant $\beta$, is investigated with special interest in its phase progression (PhasProg). The ACT-R is modeled by circular and square loops, and classified into two types: a right-handed ACT-R with positive $\beta$ and a left-handed ACT-R with negative $\beta$. Firstly, a circular ACT-R of a length of $n$ guided wavelengths is formulated. It is found that, at any depression angle $\theta$, the PhasProg with respect to azimuth angle $\phi$ is downward-sloping for the right-handed ACT-R and upward-sloping for the left-handed ACT-R. These PhasProgs have a perfectly linear change of $360n$ degrees ($n = 1, 2$) with respect to azimuth angle $\phi$. Secondly, a square ACT-R of a length of $n$ guided wavelengths is formulated. When $k_0/|\beta| = 1$ with $k_0$ being free-space phase constant, the PhasProg is found to be downward-sloping for the right-handed ACT-R and upward-sloping for the left-handed ACT-R, with a quasi-linear change of $360n$ degrees ($n = 1, 2$) with respect to azimuth angle $\phi$. Thirdly, the formulated numerical expressions are compared with simulated results obtained using natural and metaloop antennas, and reasonable agreement between these is observed. Fourthly, a comment is made on a singular phenomenon of the PhasProg for $n = 2$, with an example where $k_0/\beta = 2$.

**INDEX TERMS** Active region, radiation field, phase progression, natural loop, metaloop.

## I. INTRODUCTION

Flat antennas are classified into two groups in reference to the current distributed on the antenna conductors: resonant flat antennas and non-resonant flat antennas, where the former supports a resonant current (a standing wave current) and the latter supports a non-resonant current (a traveling wave current).

A patch antenna is a representative resonant flat antenna [1], [2]. On the other hand, a spiral antenna [3]–[8] and a curl antenna [9]–[11] are non-resonant flat antennas.

The region on the antenna conductors that is responsible for the radiation is called the active region, ACT-R. An Archimedean round (square) spiral antenna composed of two arms [3] has a circular (square) ring-shaped ACT-R whose length on the spiral conductor plane is one guided wavelength ($1\lambda_g$). This happens when the spiral arms are excited in odd mode. The current on the $1\lambda_g$ ACT-R generates a radiation beam in the direction normal to the antenna arm conductor plane, called an *axial beam*.

A round curl antenna [9] and a rectangular curl antenna [11] have a marginal structure derived from the round and rectangular Archimedean spiral antenna [3], respectively, where the number of spiral arms is reduced to one ($N_{arn} = 1$). A circular (square) ring-shaped region of length $1\lambda_g$ on the antenna arm conductor plane, where a traveling wave current is distributed, operates as the ACT-R for the round (rectangular) curl antenna to radiate an axial beam.

Round and square loop antennas with perturbation elements have a traveling wave current and form an axial beam when the loop length is $1\lambda_g$ [12], [13]. In other words, the entire loop of length $1\lambda_g$ itself operates as the ACT-R for the axial beam. Note that original round and square loop antennas [14], [15], which do not have perturbation elements, have a resonant current; this current can be changed into a non-resonant current by adding the perturbation elements.

A common characteristic of the abovementioned spiral, curl, and loop antennas is the following: an axial beam is formed by a non-resonant current (a traveling wave current)

The associate editor coordinating the review of this manuscript and approving it for publication was Neng-Wu Liu.

distributed along the ACT-R of length $1\lambda_g$ on the antenna conductor plane. It is *qualitatively* (without rigorous calculations) estimated that both of the radiation field components, $E_\theta$ and $E_\phi$, near the zenith ($\theta \approx 0°$) in the spherical coordinate system change their phase by 360° after one rotation around the antenna axis normal to the antenna conductor plane (z-axis).

Note that the two-arm spiral antenna [3] can have an ACT-R of length $2\lambda_g$ when the antenna has a peripheral length of more than $2\lambda_g$ and is excited in even mode. The radiation from the $2\lambda_g$ ACT-R is *qualitatively* estimated to be small near the antenna axis, *i.e.*, the radiation field components, $E_\theta$ and $E_\phi$, near the zenith ($\theta \approx 0°$) are small; the maximum radiation appears off the z-axis, forming a *conical beam.* Similarly, when the curl and loop antennas have a large antenna conductor to support the $2\lambda_g$ ACT-R, these antennas form a conical beam.

Recently, a technique for reducing the influence of interference waves directed toward an antenna radiating an axial beam has been discussed [16], [17]. The technique is based on transformation of the radiation pattern of the axial beam such that the radiation pattern has a null field point in the direction of the incoming interference waves. The null field point within the radiation pattern for a square metaspiral antenna [17] is realized by superimposing the conical beam produced by a $2\lambda_g$ ACT-R onto the axial beam produced by a $1\lambda_g$ ACT-R.

As mentioned above, the ACT-R for $n\lambda_g$ lengths ($n = 1, 2$) plays an important role in the formation of a radiation beam. Nevertheless, little data based on theoretical/numerical analysis of the radiation from the $n\lambda_g$ ACT-R are currently available.

Responding to this situation, this paper presents the formulated results for the radiation from the $n\lambda_g$ ACT-R ($n = 1, 2$) and focusses on the phase progression (PhasProg) of the radiation field for two cases: one is the PhasProg for a right-handed ACT-R, in which a traveling-wave current flows with a positive propagation phase constant ($\beta > 0$) and the other is the PhasProg for a left-handed ACT-R, in which a traveling-wave current flows with a negative propagation phase constant ($\beta < 0$).

This paper is composed of eight sections. Section II formulates the radiation field from a *circular* ACT-R of length $n\lambda_g$ and clarifies the behavior of the PhasProg of the radiation field. Section III formulates the radiation from a square ACT-R of length $n\lambda_g$. Based on these formulated results, Section IV discusses the phase of radiation field component $E_\theta$ for $n = 1$ with $\beta > 0$ and $\beta < 0$, followed by a discussion of the phase for the $E_\phi$ radiation field component. The discussion continues in Section V, where the following phases are clarified: $E_\theta$ for $n = 2$ with $\beta > 0$ and $\beta < 0$ and $E_\phi$ for $n = 2$ with $\beta > 0$ and $\beta < 0$. Section VI is devoted to a comparison of the formulated results with the simulated results obtained using commercially available solver CST [18]. Section VII makes a comment on a singular behavior in the PhasProg for $n = 2$ and $k_0/|\beta| = 2$, with $k_0$ ($=2\pi/\lambda_0$) being the free-space phase constant. Finally, the results obtained in this research are summarized in Section VIII.

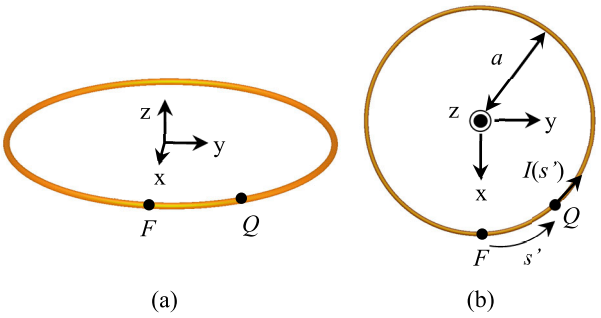


**FIGURE 1.** Circular active region (ACT-R) modeled by a circular loop. (a) Perspective view. (b) Top view.

It is worthwhile emphasizing the following points as new findings. The PhasProg of the radiation from a *circular* $n\lambda_g$ ACT-R ($n = 1, 2$) has a *perfectly linear* change of $360n$ degrees at *any* depression angle $\theta$, after one rotation around the axis of the ACT-R (z-axis). Note that the PhasProg is regressive for $\beta > 0$ and progressive for $\beta < 0$. On the other hand, the PhasProg of the radiation from a *square* $n\lambda_g$ ACT-R ($n = 1, 2$) has a *quasi-linear change*. In addition, the square ACT-R has a singular behavior when $n = 2$. As an example, it is revealed that a change from a progressive (regressive) PhasProg into a regressive (progressive) PhasProg under $k_0/|\beta| = 2$ (and hence, $|\beta|/k_0 = 0.5$) occurs when $\theta$ exceeds singular angle $\theta_S$. Such behavior is not found in the radiation from the *circular* $2\lambda_g$ ACT-R, and has not been revealed in any open literature, to the authors' best knowledge.

## II. CIRCULAR ACTIVE REGION

Fig. 1 shows a circular active region (ACT-R) modeled by a circular loop. We assume that a traveling current, $I(s')$, flows around the coordinate origin without decay, having amplitude $I_0$;

$$I(s') = I_0 e^{-j\beta s'} \tag{1}$$

where $s'$ is the distance measured along the loop from point $F$ to source point $Q$; $\beta$ ($\equiv \pm 2\pi/\lambda_g$, with $\lambda_g$ being the guided wavelength) is the propagation phase constant of the current. The ACT-R has a length of $2\pi a = n\lambda_g$, where $a$ is the radius of ACT-R. Note that $\beta$ takes positive and negative values and $n$ takes 1 and 2.

We specify a far-field point in space using spherical coordinates $(r, \theta, \phi)$. The radiation field from the loop, $\mathbf{E}(r, \theta, \phi)$, is expressed as

$$\mathbf{E}(r, \theta, \phi) = -\frac{j\omega\mu}{4\pi} \cdot \frac{e^{-jk_0 r}}{r} \int_0^{n\lambda_g} I(s')\, \hat{s}' e^{jk_0 \hat{r}\cdot\mathbf{r}'} ds', \tag{2}$$

where $\omega = 2\pi f$, with $f$ being the operating frequency; $\mu$ is the permeability; $k_0 = 2\pi/\lambda_0$ is the wave number in free space; $r$ is the distance from the coordinate origin to the far field point; $\hat{s}'$ is the unit vector tangential to the ACT-R

at source point $Q$; $\hat{r}$ is the unit vector directed toward the far-field point; $\mathbf{r}'$ is the position vector from the coordinate origin to current source point $Q$. Note that the unit vectors for spherical coordinates $(r, \theta, \phi)$ are respectively denoted as $(\hat{r}, \hat{\theta}, \hat{\phi})$ throughout this paper.

Distance $s'$, tangential unit vector $\hat{s}'$, $r$-directed unit vector $\hat{r}$, and source position vector $\mathbf{r}'$ are

$$s' = a\phi' \tag{3}$$
$$\hat{s}' = -\sin\phi'\hat{x} + \cos\phi'\hat{y} \tag{4}$$
$$\hat{r} = \sin\theta(\cos\phi\hat{x} + \sin\phi\hat{y}) + \cos\theta\hat{z} \tag{5}$$
$$\mathbf{r}' = a(\cos\phi'\hat{x} + \sin\phi'\hat{y}) \tag{6}$$

where $\phi'$ is the azimuth angle for current source point $Q$; and $\hat{x}$, $\hat{y}$, and $\hat{z}$ are the unit vectors for rectangular coordinates $x$, $y$ and $z$, respectively.

Equation (2) is written using Eqs. (1) and (3) - (6) as

$$\mathbf{E}(r,\theta,\phi) = Ca\int_0^{2n\pi} e^{-j\beta a\phi'} \cdot e^{jk_0 a\sin\theta\cos(\phi-\phi')}[-\sin\phi'\hat{x} + \cos\phi'\hat{y}]d\phi', \tag{7}$$

where $C$ is defined as

$$C \equiv \frac{-j\omega\mu}{4\pi r} I_0 e^{-jk_0 r}. \tag{8}$$

We introduce a new variable of $\psi'$ with a relationship of $\phi' = \phi - \psi'$. Then, Eq. (7) is

$$\mathbf{E}(r,\theta,\phi) = -Cae^{-j\beta a\phi}\int_{\phi}^{\phi-2n\pi} e^{j\beta a\psi'} e^{jk_0 a\sin\theta\cos\psi'} \times [-\sin(\phi-\psi')\hat{x} + \cos(\phi-\psi')\hat{y}]d\psi'. \tag{9}$$

The radiation field of Eq. (9) is decomposed into two components: $\theta$-directed component $E_\theta$ and $\phi$-directed component $E_\phi$. $E_\theta$ is written as

$$E_\theta = -Cae^{-jB_a\phi}\cos\theta\int_{\phi}^{\phi-2n\pi} h_{\sin}(\psi')d\psi', \tag{10}$$

where $B_a \equiv \beta a = +n$ for $\beta > 0$ and $-n$ for $\beta < 0$, and $h_{\sin}(\psi')$ is defined as

$$h_{\sin}(\psi') \equiv e^{jB_a\psi'} \cdot e^{jk_0 a\sin\theta\cos\psi'}\sin\psi'. \tag{11}$$

Note that the following relationship is held for $h_{\sin}(\psi')$

$$h_{\sin}(\psi') = h_{\sin}(\psi' \pm 2n\pi). \tag{12}$$

Then, Eq. (10) is written as

$$E_\theta = -Cae^{-jB_a\phi}\cos\theta\int_0^{-2n\pi} h_{\sin}(\psi')d\psi' \quad \text{for } n = 1 \text{ and } 2, \tag{13}$$

which is denoted as $E_\theta^{\mathrm{rh,n}}$ for the right-handed ACT-R with $\beta > 0$ and $E_\theta^{\mathrm{lh,n}}$ for the left-handed ACT-R with $\beta < 0$.

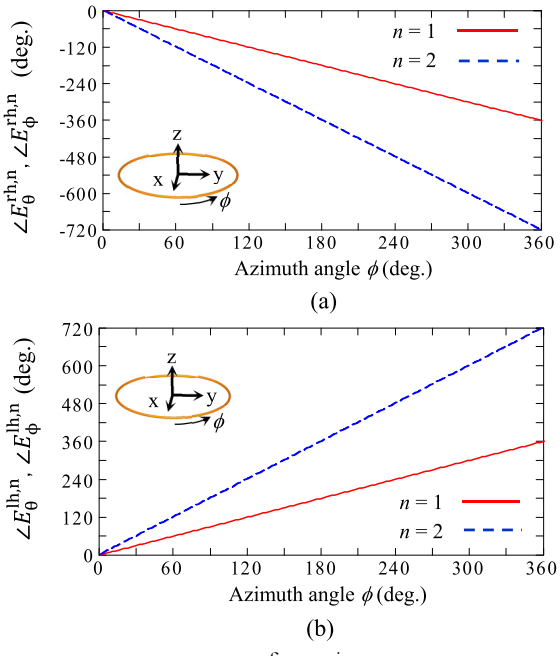


**FIGURE 2.** Standardized phase for a circular ACT-R of length $n\lambda_g$. (a) $\angle E_\theta^{\mathrm{rh,n}}$ and $\angle E_\phi^{\mathrm{rh,n}}$ for $\beta > 0$. (b) $\angle E_\theta^{\mathrm{lh,n}}$ and $\angle E_\phi^{\mathrm{lh,n}}$ for $\beta < 0$.

Similarly, $\phi$-directed component $E_\phi$ is

$$E_\phi = -Cae^{-jB_a\phi}\int_0^{-2n\pi} h_{\cos}(\psi')d\psi' \quad \text{for } n = 1 \text{ and } 2, \tag{14}$$

where

$$h_{\cos}(\psi') \equiv e^{jB_a\psi'} \cdot e^{jk_0 a\sin\theta\cos\psi'}\cos\psi', \tag{15}$$

and $E_\phi$ is denoted as $E_\phi^{\mathrm{rh,n}}$ for the right-handed ACT-R with $\beta > 0$ and $E_\phi^{\mathrm{lh,n}}$ for the left-handed ACT-R with $\beta < 0$.

It should be emphasized that the results of the integration term in Eqs. (13) and (14) do not include coordinate $\phi$, *i.e.*, they are independent of azimuth angle $\phi$. This means that the phase for radiation field components $E_\theta$ and $E_\phi$ at any azimuth angle $\phi$ is specified by $e^{-jB_a\phi}$; it follows that the phase is delayed (regressive) for $\beta > 0$ and advanced (progressive) for $\beta < 0$ with an increase in azimuth angle $\phi$. Fig. 2 shows *perfectly* linear PhasProgs of 360° for the ACT-R of length $1\lambda_g$ and 720° for the ACT-R of length $2\lambda_g$. Note that the phase at $\phi$ is standardized using the phase at $\phi = 0°$ throughout this paper: Standardized phase ≡ Phase $(\phi)$ − Phase (0°).

## III. SQUARE ACTIVE REGION

As the counterpart of a circular ACT-R, Fig. 3 shows a square ACT-R. We assume that the same current defined by Eq. (1) flows on the square ACT-R, and denote the current at the starting point for the $m^{\mathrm{th}}$ (=1, 2, 3, 4) side of the ACT-R as

$$I_0 e^{-j\beta(2l)(m-1)} \equiv I_0 c_m (\mathrm{m} = 1, 2, 3, 4), \tag{16}$$

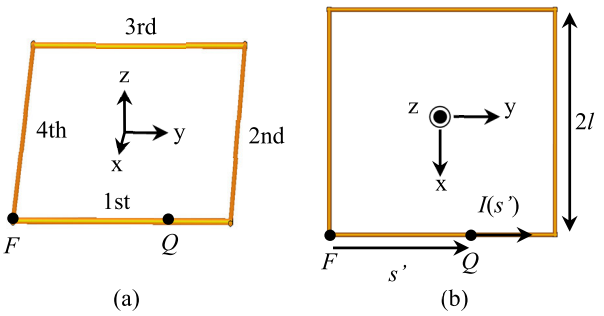


**FIGURE 3.** Square active region (ACT-R) modeled by a square loop. (a) Perspective view. (b) Top view.

where $2l$ is the side length of the ACT-R, and $8l \equiv n\lambda_g$ ($n = 1, 2$) is the total length of the ACT-R.

The radiation field generated by the current of Eq. (16) is

$$\begin{aligned}\mathbf{E}(r,\theta,\phi) &= C\int_0^{2l} c_1\hat{y}e^{-j\beta s'}\cdot e^{jk_0\mathbf{r}_1'\cdot\hat{r}}ds' \\ &+ C\int_0^{2l} c_2(-\hat{x})e^{-j\beta s'}\cdot e^{jk_0\mathbf{r}_2'\cdot\hat{r}}ds' \\ &+ C\int_0^{2l} c_3(-\hat{y})e^{-j\beta s'}\cdot e^{jk_0\mathbf{r}_3'\cdot\hat{r}}ds' \\ &+ C\int_0^{2l} c_4\hat{x}e^{-j\beta s'}\cdot e^{jk_0\mathbf{r}_4'\cdot\hat{r}}ds', \end{aligned} \tag{17}$$

where $\mathbf{r}_m'$ ($m = 1, 2, 3, 4$) denotes the position vector for a current source point located on the $m^{\text{th}}$ side of the ACT-R. The inner products of $(\mathbf{r}_m' \cdot \hat{r})$ are

$$\mathbf{r}_1'\cdot\hat{r} = \sin\theta\left\{l\cos\phi + (s'-l)\sin\phi\right\} \tag{18}$$
$$\mathbf{r}_2'\cdot\hat{r} = \sin\theta\left\{(l-s')\cos\phi + l\sin\phi\right\} \tag{19}$$
$$\mathbf{r}_3'\cdot\hat{r} = \sin\theta\left\{-l\cos\phi - (s'-l)\sin\phi\right\} \tag{20}$$
$$\mathbf{r}_4'\cdot\hat{r} = \sin\theta\left\{-(l-s')\cos\phi - l\sin\phi\right\}. \tag{21}$$

Equation (17) is transformed into

$$\begin{aligned}&\mathbf{E}(r,\theta,\phi) \\ &= \hat{y}Cc_1\frac{e^{-j\beta 2l}\cdot e^{jP} - e^{jM}}{-j\beta\left(1-\bar{k}\sin\phi\right)} - \hat{x}Cc_2\frac{e^{-j\beta 2l}\cdot e^{-jM} - e^{jP}}{-j\beta\left(1+\bar{k}\cos\phi\right)} \\ &- \hat{y}Cc_3\frac{e^{-j\beta 2l}\cdot e^{-jP} - e^{-jM}}{-j\beta\left(1+\bar{k}\sin\phi\right)} + \hat{x}Cc_4\frac{e^{-j\beta 2l}\cdot e^{jM} - e^{-jP}}{-j\beta\left(1-\bar{k}\cos\phi\right)}, \end{aligned} \tag{22}$$

where

$$\bar{k} \equiv \frac{k_0}{\beta}\sin\theta \quad (0 \le \theta \le \pi) \tag{23}$$
$$P = k_0\, l\, \sin\theta(\cos\phi + \sin\phi) \tag{24}$$
$$M = k_0\, l\, \sin\theta(\cos\phi - \sin\phi) \tag{25}$$

Note that, when $\beta$ is positive, $\bar{k}$ in Eq. (23) is positive and denoted as $\tilde{k}$; when $\beta$ is negative, $\bar{k}$ is negative and denoted as $-\tilde{k}$.

## IV. SQUARE ACTIVE REGION OF ONE GUIDED WAVELENGTH

### A. PHASE OF $E_\theta^{RH,1}$ WHERE $\beta > 0$ AND $n = 1$

We derive an equation for the $\theta$-component of the radiation field from an ACT-R of side length $2l = 1\lambda_g/4$ and positive $\beta$, *i.e.*, a right-handed square ACT-R of length $1\lambda_g$. This radiation field component is denoted as $E_\theta^{\text{RH},1}$. The values for $c_m$ in Eq. (16) are

$$(c_1, c_2, c_3, c_4) = (1, -\text{j}, -1, +\text{j}). \tag{26}$$

Using $\hat{x}\cdot\hat{\theta} = \cos\theta\cos\phi$ and $\hat{y}\cdot\hat{\theta} = \cos\theta\sin\phi$, we have $E_\theta^{\text{RH},1}$ from Eq. (22)

$$\begin{aligned}\frac{-j\beta}{C\cos\theta}E_\theta^{\text{RH},1} &= \sin\phi\frac{(-j)\cdot e^{jP} - e^{jM}}{1-\tilde{k}\sin\phi} \\ &+ j\cos\phi\frac{(-j)\cdot e^{-jM} - e^{jP}}{1+\tilde{k}\cos\phi} \\ &+ \sin\phi\frac{(-j)\cdot e^{-jP} - e^{-jM}}{1+\tilde{k}\sin\phi} \\ &+ j\cos\phi\frac{(-j)\cdot e^{jM} - e^{-jP}}{1-\tilde{k}\cos\phi}. \end{aligned} \tag{27}$$

Equation (27) is transformed into

$$\begin{aligned}\frac{-j\beta}{C\cos\theta}E_\theta^{\text{RH},1} &= \Delta_{\theta,\text{A}}^{\text{RH},1}\sin P + \Sigma_{\theta,\text{B}}^{\text{RH},1}\cos M \\ &+ j[-\Sigma_{\theta,\text{A}}^{\text{RH},1}\cos P + \Delta_{\theta,\text{B}}^{\text{RH},1}\sin M] \end{aligned} \tag{28}$$

where

$$\begin{aligned}\Sigma_{\theta,\text{A}}^{\text{RH},1} &= \frac{2(\cos\phi+\sin\phi)(1-\tilde{k}^2\cos\phi\sin\phi)}{\left(1-\tilde{k}^2\sin^2\phi\right)\left(1-\tilde{k}^2\cos^2\phi\right)} \\ &\equiv \Sigma_{\theta,\text{A}}^{\text{RH},1}\left(\tilde{k}(\theta),\phi\right) \end{aligned} \tag{29}$$

$$\begin{aligned}\Delta_{\theta,\text{A}}^{\text{RH},1} &= \frac{-2\tilde{k}(\cos^2\phi-\sin^2\phi)}{\left(1-\tilde{k}^2\sin^2\phi\right)\left(1-\tilde{k}^2\cos^2\phi\right)} \\ &\equiv \Delta_{\theta,\text{A}}^{\text{RH},1}\left(\tilde{k}(\theta),\phi\right) \end{aligned} \tag{30}$$

$$\begin{aligned}\Sigma_{\theta,\text{B}}^{\text{RH},1} &= \frac{2(\cos\phi-\sin\phi)(1+\tilde{k}^2\cos\phi\sin\phi)}{\left(1-\tilde{k}^2\sin^2\phi\right)\left(1-\tilde{k}^2\cos^2\phi\right)} \\ &= \Sigma_{\theta,\text{A}}^{\text{RH},1}\left(\tilde{k}(\theta),\phi+\frac{\pi}{2}\right) \end{aligned} \tag{31}$$

$$\begin{aligned}\Delta_{\theta,\text{B}}^{\text{RH},1} &= \frac{2\tilde{k}(\cos^2\phi-\sin^2\phi)}{\left(1-\tilde{k}^2\sin^2\phi\right)\left(1-\tilde{k}^2\cos^2\phi\right)} \\ &= \Delta_{\theta,\text{A}}^{\text{RH},1}\left(\tilde{k}(\theta),\phi+\frac{\pi}{2}\right) \end{aligned} \tag{32}$$

The phase of Eq. (28) is

$$\angle\left(\frac{-j\beta}{C\cos\theta}E_\theta^{\text{RH},1}\right) = \tan^{-1}\frac{I_\theta^{\text{RH},1}}{R_\theta^{\text{RH},1}}, \tag{33}$$

where

$$R_\theta^{\mathrm{RH},1} = 2\{-\tilde{k}\left(\cos^2\phi - \sin^2\phi\right)\sin P + (\cos\phi - \sin\phi)(1 + \tilde{k}^2\cos\phi\sin\phi) \times \cos M\} / \left\{\left(1 - \tilde{k}^2\sin^2\phi\right) \times \left(1 - \tilde{k}^2\cos^2\phi\right)\right\} \equiv R_\theta^{\mathrm{RH},1}\left(\tilde{k}(\theta), \phi\right) \quad (34)$$

$$I_\theta^{\mathrm{RH},1} = 2\{\tilde{k}\left(\cos^2\phi - \sin^2\phi\right)\sin M - (\cos\phi + \sin\phi)(1 - \tilde{k}^2\cos\phi\sin\phi) \times \cos P\} / \left\{\left(1 - \tilde{k}^2\sin^2\phi\right) \times \left(1 - \tilde{k}^2\cos^2\phi\right)\right\} \equiv I_\theta^{\mathrm{RH},1}\left(\tilde{k}(\theta), \phi\right) = R_\theta^{\mathrm{RH},1}\left(\tilde{k}(\theta), \phi + \frac{\pi}{2}\right) \quad (35)$$

Fig. 4 shows the characteristics of $E_\theta^{\mathrm{RH},1}$ as a function of azimuth angle $\phi$ with depression angle $\theta$ as a parameter, where $k_0/\beta$ is set to 1 (*i.e.*, $n\lambda_g = n\lambda_0$ with $n = 1$). It is found that the standardized phase is regressive and changes by 360° around the z-axis in an almost linear fashion.

### B. PHASE OF $E_\theta^{LH,1}$ WHERE $\beta < 0$ AND $n = 1$

Next, we derive an equation for the $\theta$-component, $E_\theta$, from a left-handed square ACT-R of length $1\lambda_g$. This $E_\theta$ is denoted as $E_\theta^{\mathrm{LH},1}$. The values for $c_m$ in Eq. (16) are set to

$$(c_1, c_2, c_3, c_4) = (1, +\mathrm{j}, -1, -\mathrm{j})\,. \quad (36)$$

Using a process similar to that used in subsection *A* leads to a relationship of

$$\frac{j|\beta|}{C\cos\theta}E_\theta^{\mathrm{LH},1} = -\Delta_{\theta,\mathrm{A}}^{\mathrm{LH},1}\sin P + \Sigma_{\theta,\mathrm{B}}^{\mathrm{LH},1}\cos M + j[\Sigma_{\theta,\mathrm{A}}^{\mathrm{LH},1}\cos P + \Delta_{\theta,\mathrm{B}}^{\mathrm{LH},1}\sin M], \quad (37)$$

where

$$\Sigma_{\theta,\mathrm{A}}^{\mathrm{LH},1} = \Sigma_{\theta,\mathrm{A}}^{\mathrm{RH},1} \quad (38)$$

$$\Delta_{\theta,\mathrm{A}}^{\mathrm{LH},1} = -\Delta_{\theta,\mathrm{A}}^{\mathrm{RH},1} \quad (39)$$

$$\Sigma_{\theta,\mathrm{B}}^{\mathrm{LH},1} = \Sigma_{\theta,\mathrm{B}}^{\mathrm{RH},1} \quad (40)$$

$$\Delta_{\theta,\mathrm{B}}^{\mathrm{LH},1} = -\Delta_{\theta,\mathrm{B}}^{\mathrm{RH},1} \quad (41)$$

Using Eq. (38) through Eq. (41), Eq. (37) is written as

$$\frac{j|\beta|}{C\cos\theta}E_\theta^{\mathrm{LH},1} = \Delta_{\theta,\mathrm{A}}^{\mathrm{RH},1}\sin P + \Sigma_{\theta,\mathrm{B}}^{\mathrm{RH},1}\cos M + j[\Sigma_{\theta,\mathrm{A}}^{\mathrm{RH},1}\cos P - \Delta_{\theta,\mathrm{B}}^{\mathrm{RH},1}\sin M]. \quad (42)$$

Note that the sign for the $j$-part in Eq. (42) is opposite to that in Eq. (28). Hence, the phase for $\frac{j|\beta|}{C\cos\theta}E_\theta^{\mathrm{LH},1}$ is written as

$$\angle\left(\frac{j|\beta|}{C\cos\theta}E_\theta^{\mathrm{LH},1}\right) = \tan^{-1}\frac{-I_\theta^{\mathrm{RH},1}}{R_\theta^{\mathrm{RH},1}} = -\angle\left(\frac{-j\beta}{C\cos\theta}E_\theta^{\mathrm{RH},1}\right). \quad (43)$$

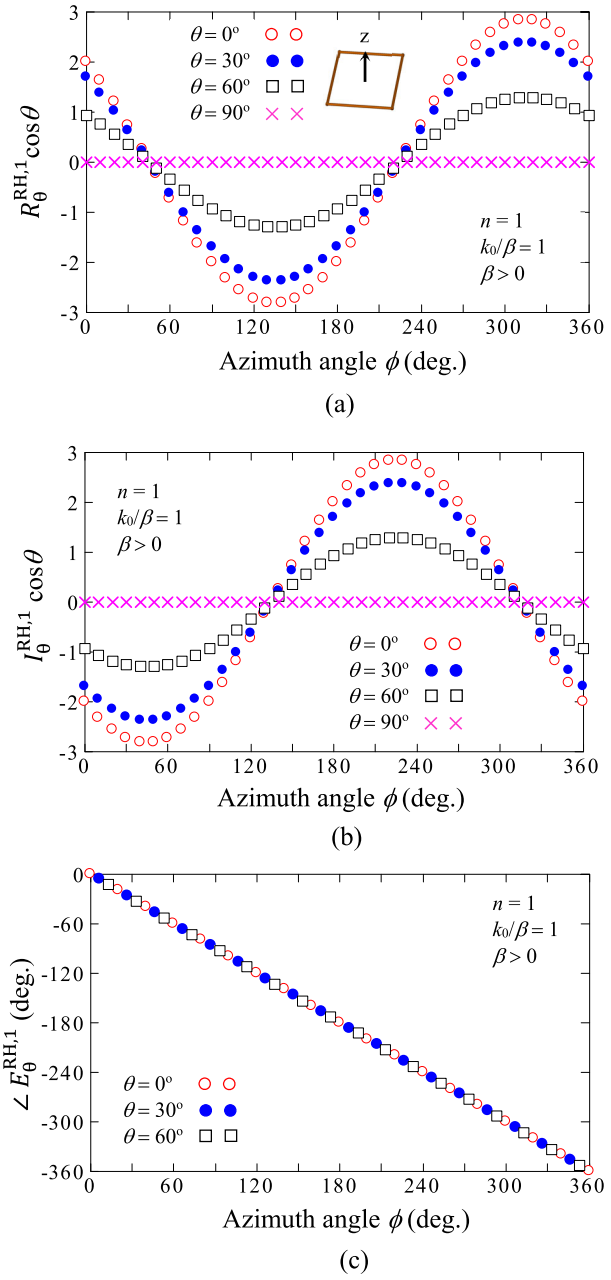


**FIGURE 4.** $E_\theta^{\mathrm{RH},1}$ from a right-handed square ACT-R of length $1\lambda_g$. (a) $R_\theta^{\mathrm{RH},1}\cos\theta$. (b) $I_\theta^{\mathrm{RH},1}\cos\theta$. (c) Standardized phase.

This means that the phase for $E_\theta^{\mathrm{LH},1}$ has an inverse characteristic to that for $E_\theta^{\mathrm{RH},1}$, *i.e.*, it is progressive (upward-sloping), as shown in Fig. 5.

### C. PHASE OF $E_\phi^{RH,1}$ WHERE $\beta > 0$ AND $n = 1$

Sections *A* and *B* have clarified the phases of the $\theta$-radiation field component for $\beta > 0$ and $\beta < 0$, where the length of the square ACT-R is set to be one guided wavelength ($n\lambda_g$ with $n = 1$). This subsection focuses on the $\phi$-radiation field component for $\beta > 0$ and $n = 1$, which is denoted as $E_\phi^{\mathrm{RH},1}$, and clarifies its phase.

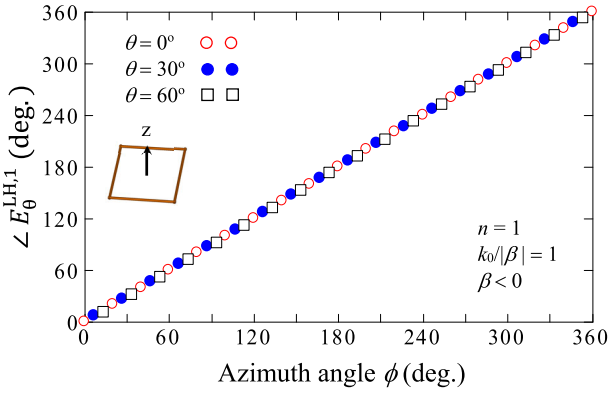


**FIGURE 5.** Standardized phase for the $\theta$-component, $E_\theta^{\mathrm{LH},1}$, of the radiation field from a left-handed square ACT-R of length $1\lambda_g$. The deviation from the perfectly linear PhasProg is less than 1°.

Using Eq. (22), we have

$$\begin{aligned}\frac{-j\beta}{C}E_\phi^{\mathrm{RH},1} &= \cos\phi\frac{(-j)\cdot e^{jP}-e^{jM}}{1-\tilde{k}\sin\phi}\\ &\quad -j\sin\phi\frac{(-j)\cdot e^{-jM}-e^{jP}}{1+\tilde{k}\cos\phi}\\ &\quad +\cos\phi\frac{(-j)\cdot e^{-jP}-e^{-jM}}{1+\tilde{k}\sin\phi}\\ &\quad -j\sin\phi\frac{(-j)\cdot e^{jM}-e^{-jP}}{1-\tilde{k}\cos\phi}. \end{aligned}\tag{44}$$

where $\hat{x}\cdot\hat{\phi}=-\sin\phi$ and $\hat{y}\cdot\hat{\phi}=\cos\phi$ are used.

Eq. (44) is reduced to

$$\begin{aligned}\frac{-j\beta}{C}E_\phi^{\mathrm{RH},1} &= -\Delta_{\phi,\mathrm{A}}^{\mathrm{RH},1}\sin P+\Sigma_{\phi,\mathrm{B}}^{\mathrm{RH},1}\cos M\\ &\quad +j[\Sigma_{\phi,\mathrm{A}}^{\mathrm{RH},1}\cos P+\Delta_{\phi,\mathrm{B}}^{\mathrm{RH},1}\sin M], \end{aligned}\tag{45}$$

where

$$\begin{aligned}\Sigma_{\phi,\mathrm{A}}^{\mathrm{RH},1} &= \frac{-2(\cos\phi-\sin\phi)(1-\tilde{k}^2\cos\phi\sin\phi-\tilde{k}^2)}{\left(1-\tilde{k}^2\sin^2\phi\right)\left(1-\tilde{k}^2\cos^2\phi\right)}\\ &\equiv \Sigma_{\phi,\mathrm{A}}^{\mathrm{RH},1}\left(\tilde{k}\,(\theta)\,,\phi\right) \end{aligned}\tag{46}$$

$$\begin{aligned}\Delta_{\phi,\mathrm{A}}^{\mathrm{RH},1} &= \frac{2\tilde{k}\left(-2+\tilde{k}^2\right)\cos\phi\sin\phi}{\left(1-\tilde{k}^2\sin^2\phi\right)\left(1-\tilde{k}^2\cos^2\phi\right)}\\ &\equiv \Delta_{\phi,\mathrm{A}}^{\mathrm{RH},1}\left(\tilde{k}\,(\theta)\,,\phi\right) \end{aligned}\tag{47}$$

$$\begin{aligned}\Sigma_{\phi,\mathrm{B}}^{\mathrm{RH},1} &= \frac{2\left(\cos\phi+\sin\phi\right)\left(-1-\tilde{k}^2\cos\phi\sin\phi+\tilde{k}^2\right)}{\left(1-\tilde{k}^2\sin^2\phi\right)\left(1-\tilde{k}^2\cos^2\phi\right)}\\ &= -\Sigma_{\phi,\mathrm{A}}^{\mathrm{RH},1}\left(\tilde{k}\,(\theta)\,,\phi+\frac{\pi}{2}\right) \end{aligned}\tag{48}$$

$$\begin{aligned}\Delta_{\phi,\mathrm{B}}^{\mathrm{RH},1} &= \frac{2\tilde{k}\left(-2+\tilde{k}^2\right)\cos\phi\sin\phi}{\left(1-\tilde{k}^2\sin^2\phi\right)\left(1-\tilde{k}^2\cos^2\phi\right)}\\ &= -\Delta_{\phi,\mathrm{A}}^{\mathrm{RH},1}\left(\tilde{k}\,(\theta)\,,\phi+\frac{\pi}{2}\right) \end{aligned}\tag{49}$$

The phase of Eq. (45) is

$$\angle\left(\frac{-j\beta}{C}E_\phi^{\mathrm{RH},1}\right)=\tan^{-1}\frac{I_\phi^{\mathrm{RH},1}}{R_\phi^{\mathrm{RH},1}},\tag{50}$$

where

$$\begin{aligned}R_\phi^{\mathrm{RH},1} &= 2\{-\tilde{k}(-2+\tilde{k}^2)\cos\phi\sin\phi\sin P\\ &\quad +(\cos\phi+\sin\phi)(-1-\tilde{k}^2\cos\phi\sin\phi+\tilde{k}^2)\cos M\}/\\ &\quad \left\{\left(1-\tilde{k}^2\sin^2\phi\right)\left(1-\tilde{k}^2\cos^2\phi\right)\right\}\\ &\equiv R_\phi^{\mathrm{RH},1}\left(\tilde{k}\,(\theta)\,,\phi\right) \end{aligned}\tag{51}$$

$$\begin{aligned}I_\phi^{\mathrm{RH},1} &= 2\{\tilde{k}(-2+\tilde{k}^2)\cos\phi\sin\phi\sin M\\ &\quad -(\cos\phi-\sin\phi)(1-\tilde{k}^2\cos\phi\sin\phi-\tilde{k}^2)\cos P\}/\\ &\quad \left\{\left(1-\tilde{k}^2\sin^2\phi\right)\left(1-\tilde{k}^2\cos^2\phi\right)\right\}\\ &= R_\phi^{\mathrm{RH},1}\left(\tilde{k}\,(\theta)\,,\phi+\frac{\pi}{2}\right) \end{aligned}\tag{52}$$

The $R_\phi^{\mathrm{RH},1}$, $I_\phi^{\mathrm{RH},1}$, and standardized phase for $E_\phi^{\mathrm{RH},1}$ for $k_0/\beta=1$ (*i.e.*, $n\lambda_g=n\lambda_0$ with $n=1$) are shown in Fig. 6. It is found that the standardized phase changes by 360° around the z-axis in an almost linear fashion.

### D. PHASE FOR $E_\phi^{LH,1}$ WHERE $\beta<0$ AND $n=1$

The phase of the $\phi$-component, $E_\phi^{\mathrm{RH},1}$, has been clarified in subsection $C$, where $\beta$ is positive. This subsection investigates $E_\phi$ for negative $\beta$, denoted as $E_\phi^{\mathrm{LH},1}$. After some manipulations, we obtain

$$\begin{aligned}\frac{j|\beta|}{C}E_\phi^{\mathrm{LH},1} &= -\Delta_{\phi,\mathrm{A}}^{\mathrm{LH},1}\sin P+\Sigma_{\phi,\mathrm{B}}^{\mathrm{LH},1}\cos M\\ &\quad +j[\Sigma_{\phi,\mathrm{A}}^{\mathrm{LH},1}\cos P+\Delta_{\phi,\mathrm{B}}^{\mathrm{LH},1}\sin M], \end{aligned}\tag{53}$$

where

$$\Sigma_{\phi,\mathrm{A}}^{\mathrm{LH},1}=-\Sigma_{\phi,\mathrm{A}}^{\mathrm{RH},1}\tag{54}$$

$$\Delta_{\phi,\mathrm{A}}^{\mathrm{LH},1}=\Delta_{\phi,\mathrm{A}}^{\mathrm{RH},1}\tag{55}$$

$$\Sigma_{\phi,\mathrm{B}}^{\mathrm{LH},1}=\Sigma_{\phi,\mathrm{B}}^{\mathrm{RH},1}\tag{56}$$

$$\Delta_{\phi,\mathrm{B}}^{\mathrm{LH},1}=-\Delta_{\phi,\mathrm{B}}^{\mathrm{RH},1}\tag{57}$$

Therefore, Eq. (53) is written as

$$\begin{aligned}\frac{j|\beta|}{C}E_\phi^{\mathrm{LH},1} &= -\Delta_{\phi,\mathrm{A}}^{\mathrm{RH},1}\sin P+\Sigma_{\phi,\mathrm{B}}^{\mathrm{RH},1}\cos M\\ &\quad -j[\Sigma_{\phi,\mathrm{A}}^{\mathrm{RH},1}\cos P+\Delta_{\phi,\mathrm{B}}^{\mathrm{RH},1}\sin M], \end{aligned}\tag{58}$$

Comparing Eq. (58) with Eq. (45), we have the following relationship for the phase.

$$\angle\left(\frac{j|\beta|}{C}E_\phi^{\mathrm{LH},1}\right)=-\angle\left(\frac{-j\beta}{C}E_\phi^{\mathrm{RH},1}\right)\tag{59}$$

It follows that the PhasProgs for $E_\phi^{\mathrm{LH},1}$ and $E_\phi^{\mathrm{RH},1}$ are the same except for their gradient: upward-sloping for $E_\phi^{\mathrm{LH},1}$, as shown in Fig. 7, and downward-sloping for $E_\phi^{\mathrm{RH},1}$, as shown in Fig. 6(c).

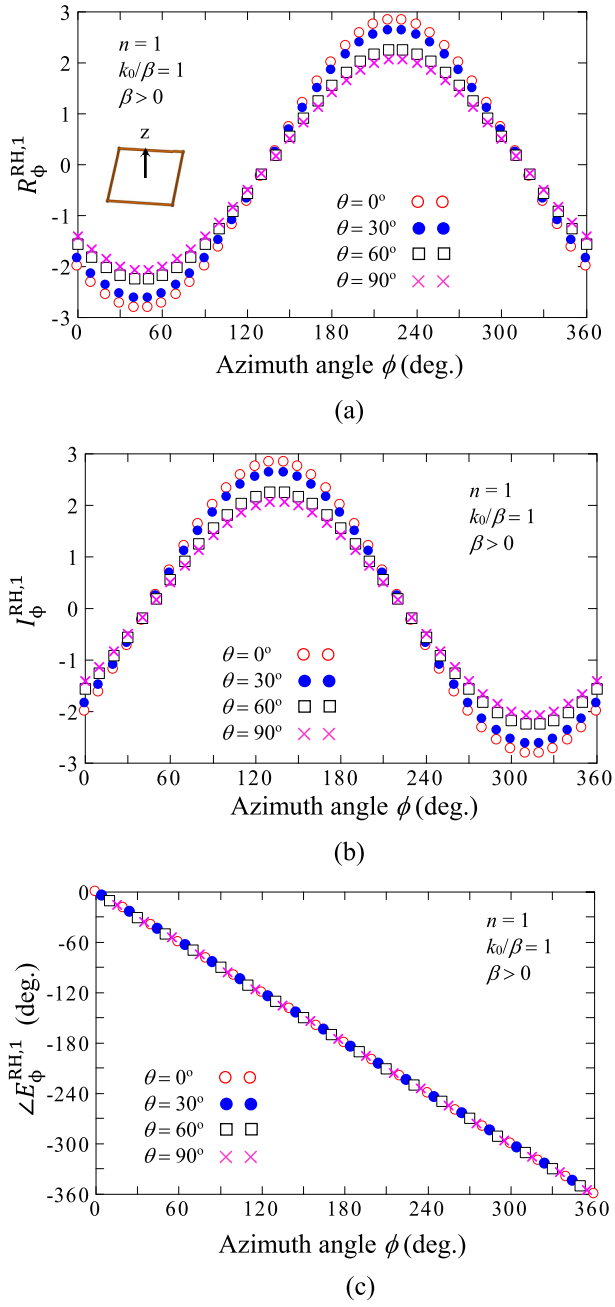


**FIGURE 6.** $E_\phi^{\mathrm{RH},1}$ from a right-handed square ACT-R of length $1\lambda_g$. (a) $R_\phi^{\mathrm{RH},1}$. (b) $I_\phi^{\mathrm{RH},1}$. (c) Standardized phase.

## V. SQUARE ACTIVE REGION OF TWO GUIDED WAVELENGTHS

### A. PHASE FOR $E_\theta^{RH,2}$ WHERE $\beta > 0$ AND $n = 2$

In this subsection, the radiation field from a square ACT-R whose length is two guided wavelengths ($8l = n\lambda_g$, with $n = 2$) is formulated to reveal the phase around the z-axis, where the propagation phase constant is set to be positive: $\beta > 0$. The values of $c_m$ (m = 1, 2, 3, 4) in Eq. (16) are set to

$$(c_1, c_2, c_3, c_4) = (1, -1, 1, -1)\,. \tag{60}$$

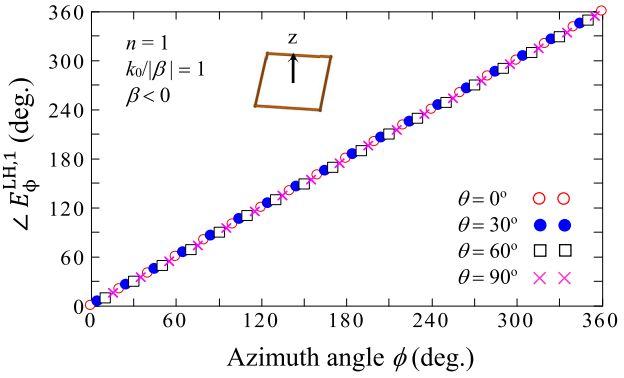


**FIGURE 7.** Standardized phase for $E_\phi^{\mathrm{LH},1}$ from a left-handed square ACT-R of length $1\lambda_g$.

The $\theta$-component of the radiation field for $n = 2$, denoted as $E_\theta^{\mathrm{RH},2}$, is obtained from Eq. (22).

$$\frac{-j\beta}{C\cos\theta}E_\theta^{\mathrm{RH},2} = \Sigma_{\theta,\mathrm{A}}^{\mathrm{RH},2}\cos P + \Sigma_{\theta,\mathrm{B}}^{\mathrm{RH},2}\cos M + j[\Delta_{\theta,\mathrm{A}}^{\mathrm{RH},2}\sin P + \Delta_{\theta,\mathrm{B}}^{\mathrm{RH},2}\sin M], \tag{61}$$

where

$$\Sigma_{\theta,\mathrm{A}}^{\mathrm{RH},2} = \frac{2\tilde{k}\left(\cos^2\phi - \sin^2\phi\right)}{\left(1-\tilde{k}^2\sin^2\phi\right)\left(1-\tilde{k}^2\cos^2\phi\right)} \tag{62}$$

$$\Delta_{\theta,\mathrm{A}}^{\mathrm{RH},2} = \frac{-2\left(\cos\phi + \sin\phi\right)\left(1-\tilde{k}^2\cos\phi\sin\phi\right)}{\left(1-\tilde{k}^2\sin^2\phi\right)\left(1-\tilde{k}^2\cos^2\phi\right)} \tag{63}$$

$$\Sigma_{\theta,\mathrm{B}}^{\mathrm{RH},2} = \frac{2\tilde{k}\left(\cos^2\phi - \sin^2\phi\right)}{\left(1-\tilde{k}^2\sin^2\phi\right)\left(1-\tilde{k}^2\cos^2\phi\right)} \tag{64}$$

$$\Delta_{\theta,\mathrm{B}}^{\mathrm{RH},2} = \frac{2\left(\cos\phi - \sin\phi\right)\left(1+\tilde{k}^2\cos\phi\sin\phi\right)}{\left(1-\tilde{k}^2\sin^2\phi\right)\left(1-\tilde{k}^2\cos^2\phi\right)} \tag{65}$$

Therefore, the following phase relationship is obtained.

$$\angle\left(\frac{-j\beta}{C\cos\theta}E_\theta^{\mathrm{RH},2}\right) = \tan^{-1}\frac{I_\theta^{\mathrm{RH},2}}{R_\theta^{\mathrm{RH},2}} \tag{66}$$

where

$$R_\theta^{\mathrm{RH},2} = 2\tilde{k}\left(\cos^2\phi - \sin^2\phi\right)(\cos P + \cos M) \Big/ \left\{\left(1-\tilde{k}^2\sin^2\phi\right)\left(1-\tilde{k}^2\cos^2\phi\right)\right\} \tag{67}$$

$$I_\theta^{\mathrm{RH},2} = -2\{(\cos\phi + \sin\phi)\left(1-\tilde{k}^2\cos\phi\sin\phi\right)\sin P - (\cos\phi - \sin\phi)\left(1+\tilde{k}^2\cos\phi\sin\phi\right)\sin M\} \Big/ \left\{\left(1-\tilde{k}^2\sin^2\phi\right)\left(1-\tilde{k}^2\cos^2\phi\right)\right\} \tag{68}$$

Fig. 8 shows the characteristics of $E_\theta^{\mathrm{RH},2}$, where $k_0/\beta = 1$ (and hence, loop length $2\lambda_g = 2\lambda_0$) is chosen as an example. It is found that both real part $R_\theta^{\mathrm{RH},2}$ and imaginary part $I_\theta^{\mathrm{RH},2}$ have two maximum values and two minimum values around the z-axis. This brings a phase change of 720° around the z-axis, as shown in Fig. 8(c), *i.e.*, the change in the phase is double of that for a square ACT-R of length $1\lambda_g$. It is found

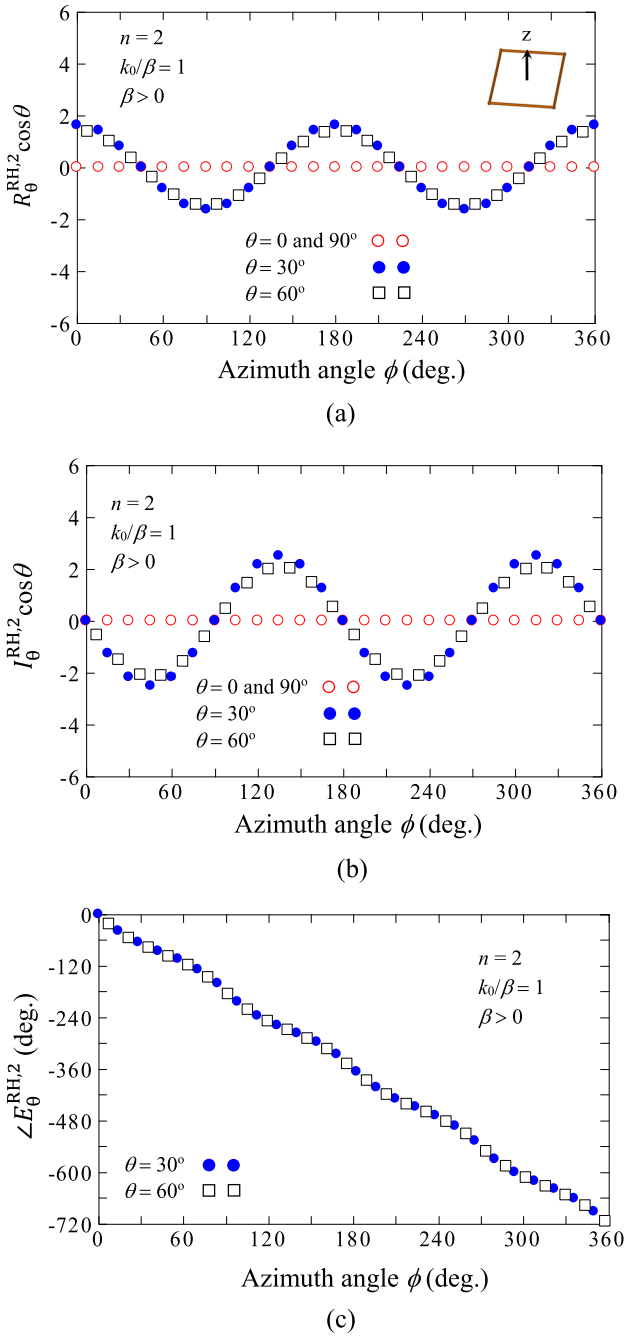


**FIGURE 8.** $E_\theta^{\mathrm{RH},2}$ **from a right-handed square ACT-R of length** $2\lambda_g$**.** **(a)** $R_\theta^{\mathrm{RH},2}\cos\theta$**. (b)** $I_\theta^{\mathrm{RH},2}\cos\theta$**. (c) Standardized phase.**

that the PhasProg does not have a perfectly linear change with increase in azimuth angle $\phi$.

### B. PHASE OF $E_\theta^{LH,2}$ WHERE $\beta < 0$ AND $n = 2$

We denote radiation field component $E_\theta$ for $n = 2$ and negative $\beta$ as $E_\theta^{\mathrm{LH},2}$, which is formulated by starting from Eq. (22), where $c_{\mathrm{m}}$ $(m = 1, 2, 3, 4)$ is

$$(c_1, c_2, c_3, c_4) = (1, -1, 1, -1)\,. \tag{69}$$

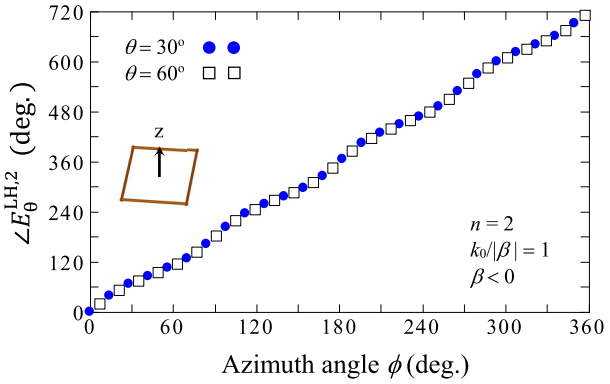


**FIGURE 9.** $E_\theta^{\mathrm{LH},2}$ **from a left-handed square ACT-R of length** $2\lambda_g$**.**

Eq. (69) is the same as Eq. (60). Eq. (22) is transformed into

$$\frac{j|\beta|}{C\cos\theta}E_\theta^{\mathrm{LH},2} = \Sigma_{\theta,\mathrm{A}}^{\mathrm{LH},2}\cos P + \Sigma_{\theta,\mathrm{B}}^{\mathrm{LH},2}\cos M + j[\Delta_{\theta,\mathrm{A}}^{\mathrm{LH},2}\sin P + \Delta_{\theta,\mathrm{B}}^{\mathrm{LH},2}\sin M], \tag{70}$$

where

$$\Sigma_{\theta,\mathrm{A}}^{\mathrm{LH},2} = \Sigma_{\theta,\mathrm{A}}^{\mathrm{RH},2} \tag{71}$$
$$\Sigma_{\theta,\mathrm{B}}^{\mathrm{LH},2} = \Sigma_{\theta,\mathrm{B}}^{\mathrm{RH},2} \tag{72}$$
$$\Delta_{\theta,\mathrm{A}}^{\mathrm{LH},2} = -\Delta_{\theta,\mathrm{A}}^{\mathrm{RH},2} \tag{73}$$
$$\Delta_{\theta,\mathrm{B}}^{\mathrm{LH},2} = -\Delta_{\theta,\mathrm{B}}^{\mathrm{RH},2} \tag{74}$$

As a result, the phase relationship is

$$\angle\left(\frac{j|\beta|}{C\cos\theta}E_\theta^{\mathrm{LH},2}\right) = \tan^{-1}\frac{-I_\theta^{\mathrm{RH},2}}{R_\theta^{\mathrm{RH},2}} = -\angle\left(\frac{-j\beta}{C\cos\theta}E_\theta^{\mathrm{RH},2}\right) \tag{75}$$

This means that the standardized phase for $E_\theta^{\mathrm{LH},2}$ is obtained by changing the downward-sloping curve for $E_\theta^{\mathrm{RH},2}$ in Fig. 8(c) into an upward-sloping curve, as shown in Fig. 9.

### C. PHASE FOR $E_\phi^{RH,2}$ WHERE $\beta > 0$ AND $n = 2$

We derive $\phi$-component $E_\phi$ from a square ACT-R of length $2\lambda_{\mathrm{g}}$ and positive $\beta$, denoted as $E_\phi^{\mathrm{RH},2}$, using the same process as that used in subsection *A*.

$$\frac{-j\beta}{C}E_\phi^{\mathrm{RH},2} = \Sigma_{\phi,\mathrm{A}}^{\mathrm{RH},2}\cos P + \Sigma_{\phi,\mathrm{B}}^{\mathrm{RH},2}\cos M + j[\Delta_{\phi,\mathrm{A}}^{\mathrm{RH},2}\sin P + \Delta_{\phi,\mathrm{B}}^{\mathrm{RH},2}\sin M], \tag{76}$$

where

$$\Sigma_{\phi,\mathrm{A}}^{\mathrm{RH},2} = \frac{-2\tilde{k}\left(2-\tilde{k}^2\right)\cos\phi\sin\phi}{(1-\tilde{k}^2\sin^2\phi)(1-\tilde{k}^2\cos^2\phi)} \tag{77}$$

$$\Delta_{\phi,\mathrm{A}}^{\mathrm{RH},2} = \frac{-2(\cos\phi-\sin\phi)(1-\tilde{k}^2\cos\phi\sin\phi-\tilde{k}^2)}{(1-\tilde{k}^2\sin^2\phi)(1-\tilde{k}^2\cos^2\phi)} \equiv \Delta_{\phi,\mathrm{A}}^{\mathrm{RH},2}\left(\tilde{k}\,(\theta)\,,\phi\right) \tag{78}$$

$$\Sigma_{\phi,\mathrm{B}}^{\mathrm{RH},2} = \Sigma_{\phi,\mathrm{A}}^{\mathrm{RH},2} \tag{79}$$

$$\begin{aligned}\Delta_{\phi,\mathrm{B}}^{\mathrm{RH},2} &= \frac{-2(\cos\phi+\sin\phi)(1+\tilde{k}^2\cos\phi\sin\phi-\tilde{k}^2)}{\left(1-\tilde{k}^2\sin^2\phi\right)\left(1-\tilde{k}^2\cos^2\phi\right)} \\ &= -\Delta_{\phi,\mathrm{A}}^{\mathrm{RH},2}\left(\tilde{k}\,(\theta)\,,\phi+\frac{\pi}{2}\right)\end{aligned} \tag{80}$$

Therefore, the phase relationship is

$$\angle\left(\frac{-j\beta}{C}E_\phi^{\mathrm{RH},2}\right) = \tan^{-1}\frac{I_\phi^{\mathrm{RH},2}}{R_\phi^{\mathrm{RH},2}}, \tag{81}$$

where

$$\begin{aligned}R_\phi^{\mathrm{RH},2} &= -2\tilde{k}\left(2-\tilde{k}^2\right)\cos\phi\sin\phi(\cos P+\cos M)/ \\ &\quad\left\{\left(1-\tilde{k}^2\sin^2\phi\right)\left(1-\tilde{k}^2\cos^2\phi\right)\right\}\end{aligned} \tag{82}$$

$$\begin{aligned}I_\phi^{\mathrm{RH},2} &= -2\{(1-\tilde{k}^2\cos\phi\sin\phi-\tilde{k}^2)(\cos\phi-\sin\phi)\sin P \\ &\quad+(1+\tilde{k}^2\cos\phi\sin\phi-\tilde{k}^2)(\cos\phi+\sin\phi)\sin M\}/ \\ &\quad\left\{\left(1-\tilde{k}^2\sin^2\phi\right)\left(1-\tilde{k}^2\cos^2\phi\right)\right\}\end{aligned} \tag{83}$$

Fig. 10 shows radiation field component $E_\phi^{\mathrm{RH},2}$ and its standardized phase for $k_0/\beta = 1$. It is found that there is a nonlinear phase change of 720° with an azimuth angle change of 360°.

### D. PHASE FOR $E_\phi^{LH,2}$ WHERE $\beta < 0$ AND $n = 2$

The $\phi$-component of the radiation field from a square ACT-R of length $2\lambda_g$ and negative $\beta$, $E_\phi^{\mathrm{LH},2}$, is derived from Eq. (22).

$$\begin{aligned}\frac{j|\beta|}{C}E_\phi^{\mathrm{LH},2} &= -\Delta_{\phi,\mathrm{B}}^{\mathrm{LH},2}\cos P-\Delta_{\phi,\mathrm{A}}^{\mathrm{LH},2}\cos M \\ &\quad+j[-\Sigma_{\phi,\mathrm{B}}^{\mathrm{LH},2}\sin P-\Sigma_{\phi,\mathrm{A}}^{\mathrm{LH},2}\sin M],\end{aligned} \tag{84}$$

where

$$\Sigma_{\phi,\mathrm{A}}^{\mathrm{LH},2} = -\Delta_{\phi,\mathrm{B}}^{\mathrm{RH},2} \tag{85}$$

$$\Delta_{\phi,\mathrm{A}}^{\mathrm{LH},2} = \Sigma_{\phi,\mathrm{B}}^{\mathrm{RH},2} \tag{86}$$

$$\Sigma_{\phi,\mathrm{B}}^{\mathrm{LH},2} = -\Delta_{\phi,\mathrm{A}}^{\mathrm{RH},2} \tag{87}$$

$$\Delta_{\phi,\mathrm{B}}^{\mathrm{LH},2} = \Sigma_{\phi,\mathrm{A}}^{\mathrm{RH},2} \tag{88}$$

Therefore, Eq. (84) is written as

$$\begin{aligned}\frac{j|\beta|}{C}E_\phi^{\mathrm{LH},2} &= -\Sigma_{\phi,\mathrm{A}}^{\mathrm{RH},2}\cos P-\Sigma_{\phi,\mathrm{B}}^{\mathrm{RH},2}\cos M \\ &\quad+j[\Delta_{\phi,\mathrm{A}}^{\mathrm{RH},2}\sin P+\Delta_{\phi,\mathrm{B}}^{\mathrm{RH},2}\sin M],\end{aligned} \tag{89}$$

The phase relationship is

$$\begin{aligned}\angle\left(\frac{j|\beta|}{C}E_\phi^{\mathrm{LH},2}\right) &= \tan^{-1}\frac{I_\phi^{\mathrm{RH},2}}{-R_\phi^{\mathrm{RH},2}} \\ &= -\angle\left(\frac{-j\beta}{C}E_\phi^{\mathrm{RH},2}\right)\end{aligned} \tag{90}$$

The gradient of the PhasProg for $E_\phi^{\mathrm{LH},2}$ is the inverse of that for $E_\phi^{\mathrm{RH},2}$. Fig. 11 shows standardized phase $E_\phi^{\mathrm{LH},2}$ for

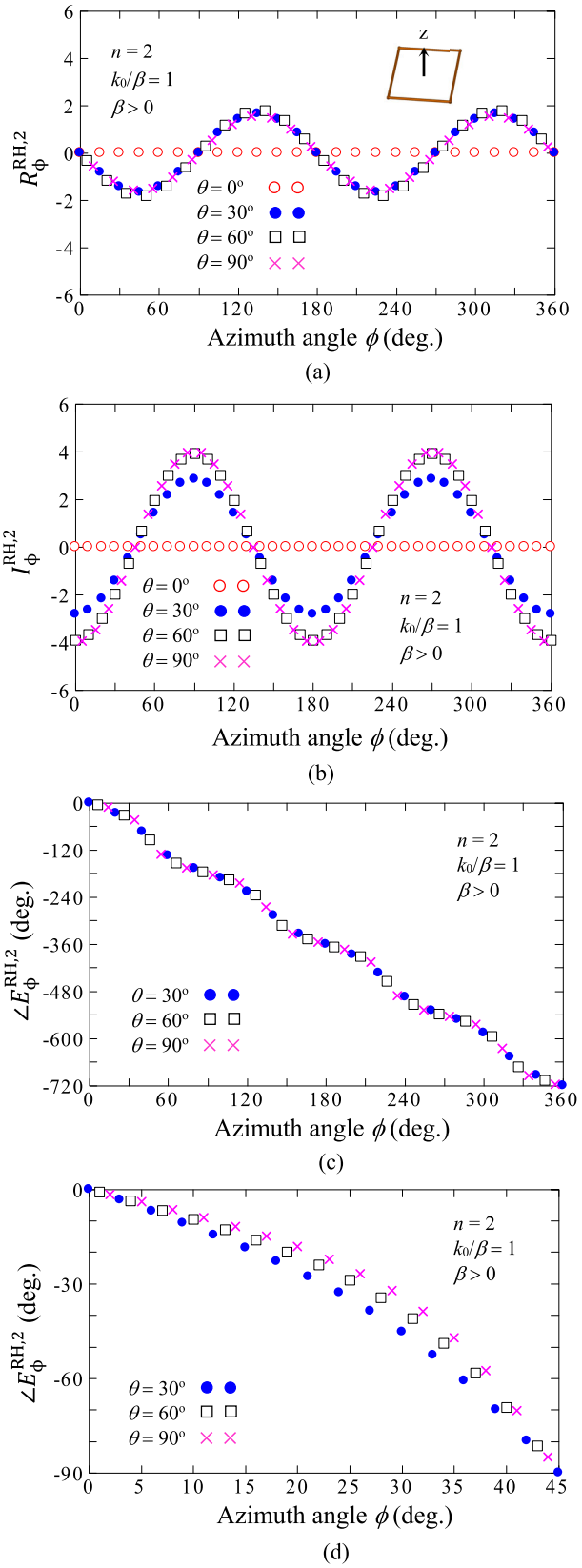


**FIGURE 10.** $E_\phi^{\mathrm{RH},2}$ from a right-handed square ACT-R of length $2\lambda_g$. (a) $R_\phi^{\mathrm{RH},2}$. (b) $I_\phi^{\mathrm{RH},2}$. (c) Standardized phase. (d) Partial expansion for (c).

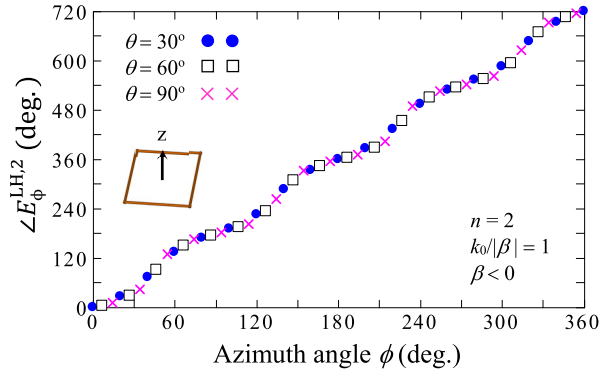


**FIGURE 11.** Standardized phase of $E_{\phi}^{\mathrm{LH},2}$ from a left-handed square ACT-R of length $2\lambda_{\mathrm{g}}$.

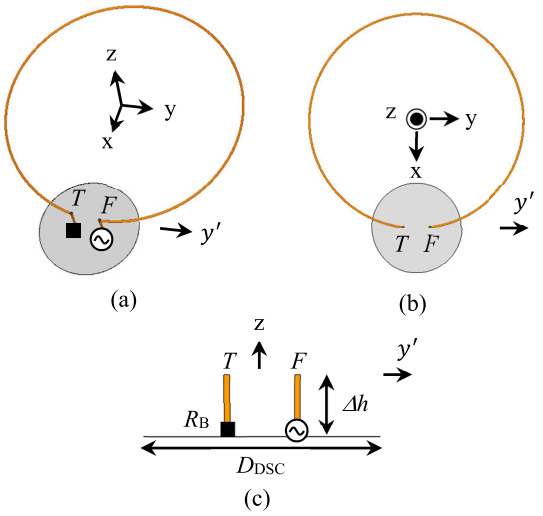


**FIGURE 12.** Round natural loop antenna (model of a right-handed circular ACT-R). (a) Perspective view. (b) Top view. (c) Side view.

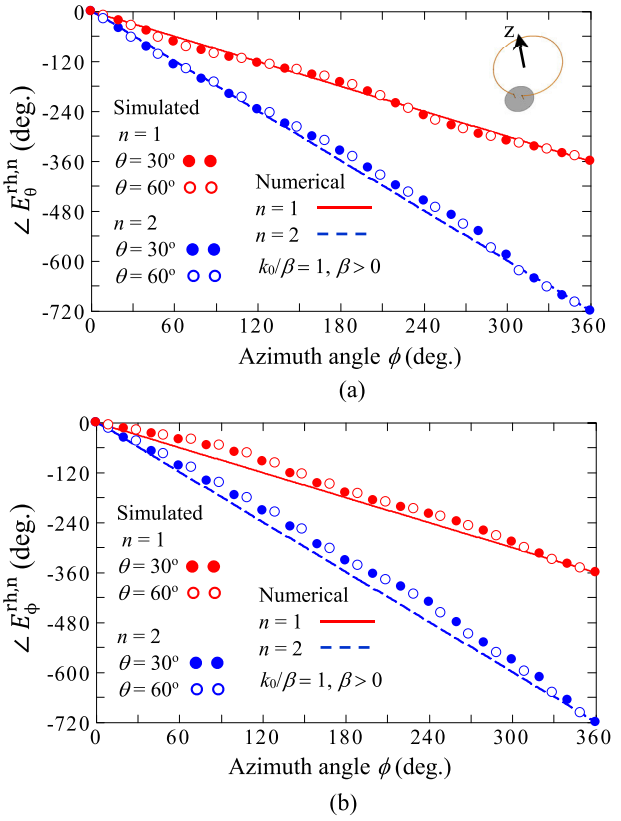


**FIGURE 13.** Simulated standardized phase of the radiation field from the round natural loop antenna (model of a right-handed circular ACT-R). The simulation is performed at $f = 2.0$ GHz, where $k_0/\beta = 1$ (and hence loop length $n\lambda_{\mathrm{g}} = n\lambda_0$) is approximately realized. (a) $\angle E_{\theta}^{\mathrm{rh,n}}$, where $n = 1$ and 2 (b) $\angle E_{\phi}^{\mathrm{rh,n}}$, where $n = 1$ and 2.

$k_0/|\beta| = 1$, which non-linearly changes by 720° around the z-axis with an upward-sloping PhasProg.

Note that, as an example, the PhasProg in Sections IV and V is presented for $k_0/|\beta| = 1$ (and hence loop length $n\lambda_{\mathrm{g}} = n\lambda_0$), which reveals a regressive PhasProg for $\beta > 0$ and a progressive PhasProg for $\beta < 0$. This trend also holds for $k_0/|\beta| = 2$ (and hence loop length $n\lambda_{\mathrm{g}} = 2n\lambda_0$). Later, in Section VII, a singular behavior in the PhasProg will be discussed.

## VI. COMPARISON

The numerical/formulated results obtained in Section II through Section V are compared with simulated results obtained using CST [18].

### A. PHASE OF THE RADIATION FIELD FROM A CIRCULAR ACT-R

For comparison with Eq. (13) and Eq. (14), *i.e.*, Fig. 2, a round conducting wire loop (natural loop with $\beta > 0$), shown in Fig. 12, is used to approximate a circular ACT-R of length $n\lambda_{\mathrm{g}}$. The loop is excited at point $F$, at a height of $\Delta h = 5.0$ mm from a small conducting disc, and terminated with a resistive load of $R_{\mathrm{B}} = 200$ ohms between the disc and the bottom of point $T$. The diameter of the disc supporting the feed and termination, $D_{\mathrm{DSC}}$, is chosen to be small to minimize the effect on the current distribution of the round loop: $D_{\mathrm{DSC}} = 20$ mm. Simulation is performed using a frequency of $f = 2.0$ GHz, a wire diameter of $2a_{\mathrm{wire}} = 0.5$ mm, and a loop circumference of $n\lambda_{\mathrm{g}} \approx n\lambda_0 = 150n$ mm.

Fig. 13 shows simulation results for depression angles $\theta = 30°$ and 60°. It is found that the simulation results for the right-handed ACT-R (where $\beta$ is positive) have a downward-sloping phase change of 360° for $n = 1$, although a perfectly linear change is not obtained due to the influence of the small disc. It is also found that the simulation results have a downward-sloping phase change of 720° for $n = 2$.

Note that a left-handed circular ACT-R, where a travelling wave current flows with *negative* $\beta$, is not supported by the *natural* loop antenna shown in Fig. 12. However, the round *metaloop* antenna shown in Fig. 14, composed of $C$-type metaatoms (CRLH transmission line cells [19], [20]), approximately realizes a left-handed circular ACT-R, where an infinitely extended ground plane at $z = -B$ is removed

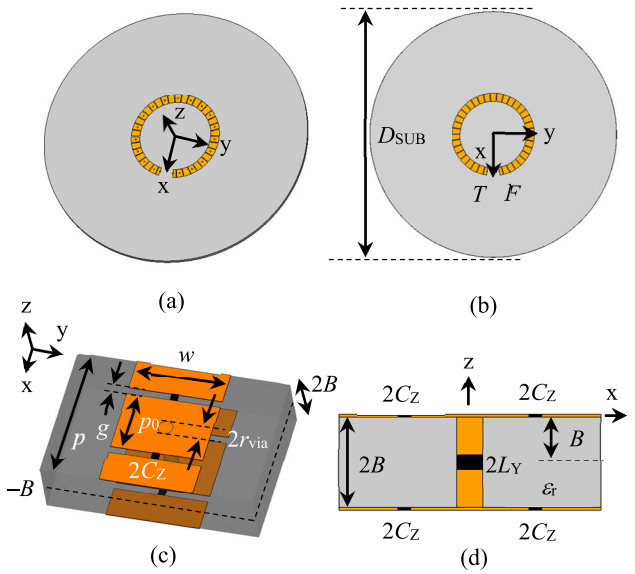


**FIGURE 14.** Round metaloop antenna as a model of the left-handed circular ACT-R. (a) Perspective view. (b) Top view. (c) Perspective view of the *C*-type metaatom. (d) Side view of the *C*-type metaatom.

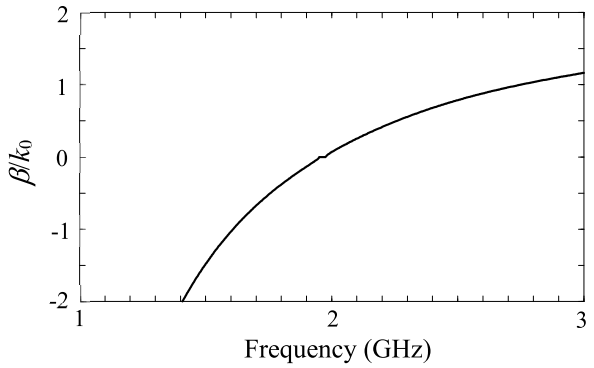


**FIGURE 15.** Dispersion diagram for the *C*-type metaatom.

**TABLE 1.** Parameters for the round metaloop.

| Symbol | Value | Symbol | Value |
|---|---|---|---|
| $2B$ | 3.2 mm | $\varepsilon_r$ | 2.6 |
| $p$ | 10.0 mm | $p_0$ | 4.5 mm |
| $g$ | 0.5 mm | $w$ | 6.6 mm |
| $2r_{via}$ | 1.0 mm | $2C_Z$ | 4.0 pF |
| $2L_Y$ | 8.0 nH | $2R_B$ | 120 Ω |
| $D_{SUB}$ | 300 mm | | |

using image theory. Using this model, the phase of the radiation field from the round metaloop antenna is simulated. The parameters used for the simulation are summarized in Table 1 and the dispersion for the *C*-type metaatom is shown in Fig. 15. Note that the standardized phase due to the upper and lower currents is the same as that due to the upper current (see Appendix A).

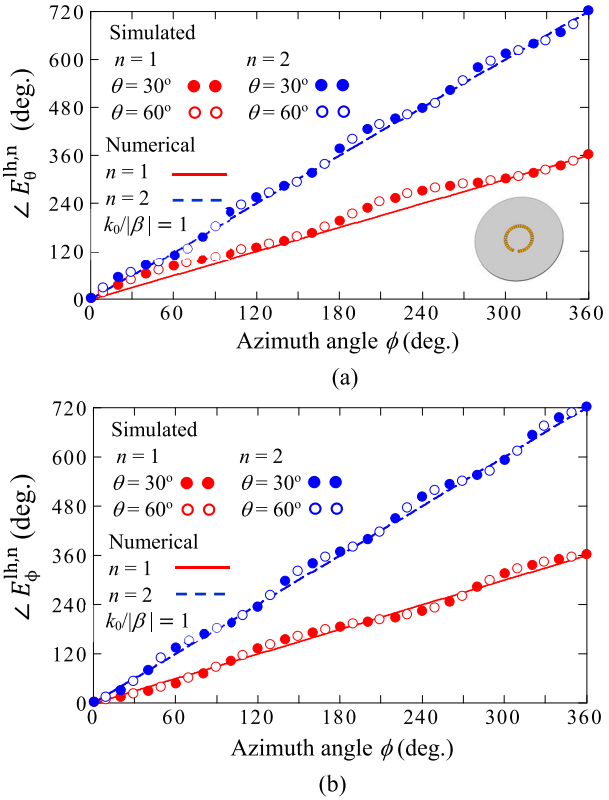


**FIGURE 16.** Simulated standardized phase of the radiation field from the round metaloop antenna (model of a left-handed circular ACT-R). The simulation is performed at $f = 1.61$ GHz, where $k_0/|\beta| = 1$ (and hence loop length $n\lambda_g = n\lambda_0$) is approximately obtained in the dispersion diagram. (a) $\angle E_\theta^{lh,n}$, where $n = 1$ and 2. (b) $\angle E_\phi^{lh,n}$, where $n = 1$ and 2.

Figs. 16 (a) and (b) show the phase of the radiation from the left-handed circular ACT-R ($\beta$ is negative) at 1.61 GHz, where $k_0/|\beta| = 1$ (and hence loop length $n\lambda_g = n\lambda_0$) is approximately realized in Fig. 15. It is found that simulation results provide the same behavior shown in Fig. 2(b), where *progressive* phase changes of 360° for $n = 1$ and 720° for $n = 2$ around the z-axis are produced.

### *B. PHASE OF THE RADIATION FIELD FROM A SQUARE ACT-R*

As a model of a right-handed square ACT-R, the square *natural* loop shown in Fig. 17 is excited from point $F$ using a frequency $f = 2.0$ GHz. The parameters used are as follows: wire diameter $2a_{wire} = 0.5$ mm, resistive load $R_B = 200$ ohms, disc diameter $D_{DSC} = 20$ mm, and height $\Delta h = 5$ mm. The loop length including the gap between points $F$ and $T$ is set to be 150 mm for $n = 1$ and 300 mm for $n = 2$. These parameters are the same as those used for the round natural loop antenna.

Fig. 18 shows simulation results for $\theta = 30°$ and 60°, which are found to agree with the numerical results, having regressive phase changes of 360° for $n = 1$ and 720° for $n = 2$.

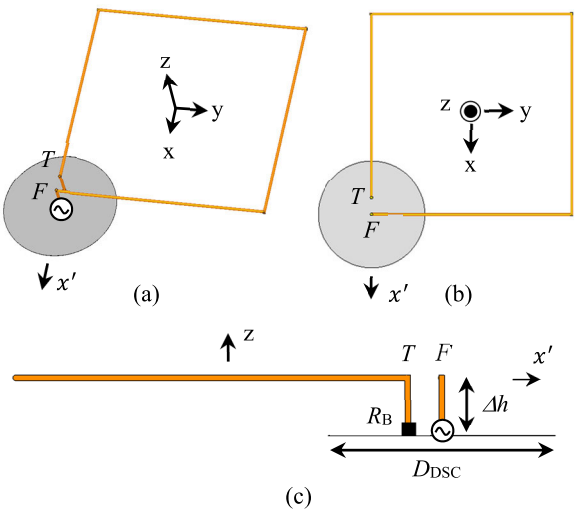


**FIGURE 17.** Square natural loop antenna (model of a right-handed square ACT-R). (a) Perspective view. (b) Top view. (c) Side view.

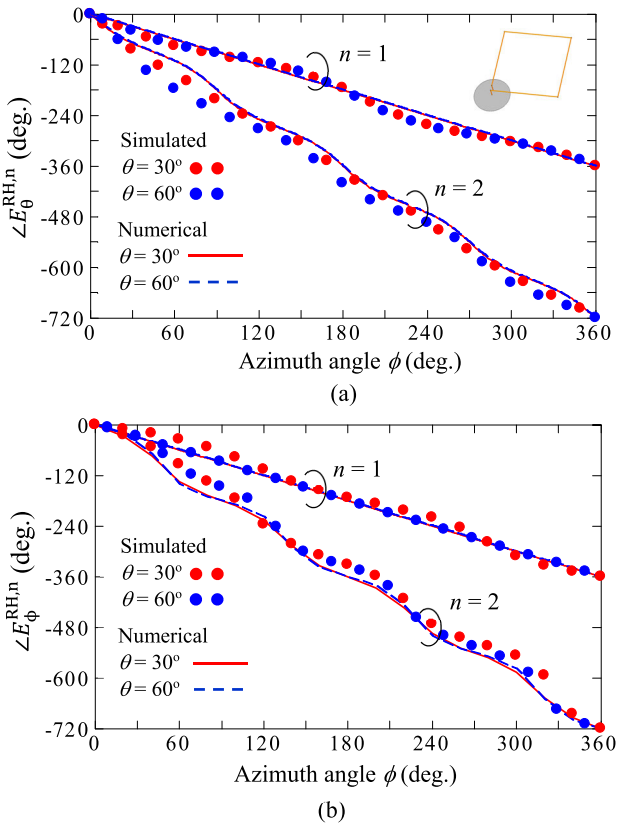


**FIGURE 18.** Simulated standardized phase of the radiation field from the square natural loop antenna (model of a right-handed square ACT-R). The simulation is performed at $f = 2.0$ GHz, where $k_0/\beta = 1$ (and hence loop length $n\lambda_g = n\lambda_0$) is approximately realized. (a) $\angle E_\theta^{RH,n}$, where $n = 1$ and 2. (b) $\angle E_\phi^{RH,n}$, where $n = 1$ and 2.

The square *natural* loop antenna shown in Fig. 17 cannot produce a left-handed square ACT-R, which has a travelling wave current with *negative* $\beta$. Therefore, we use a

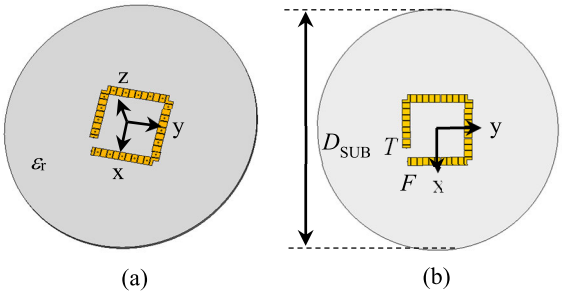


**FIGURE 19.** Square metaloop antenna as a model of the left-handed square ACT-R. (a) Perspective view. (b) Top view.

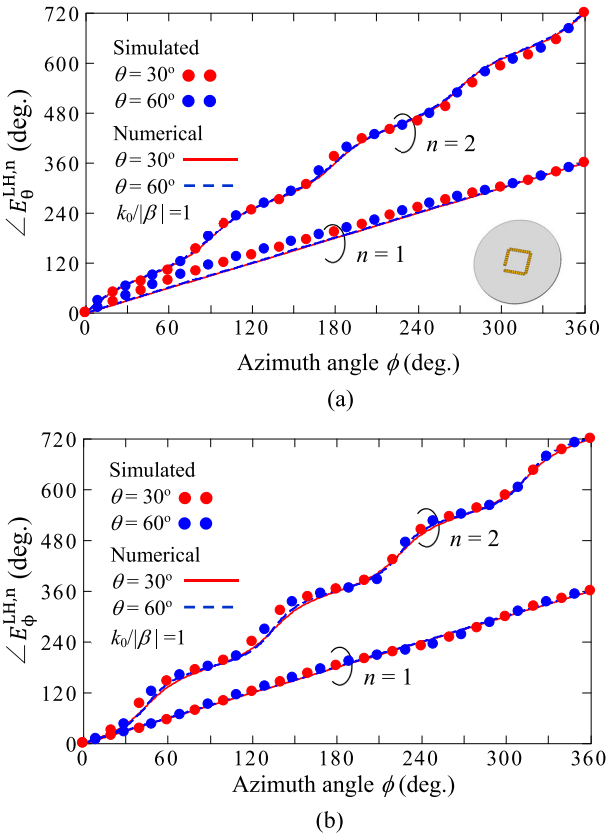


**FIGURE 20.** Simulated standardized phase of the radiation field from the square metaloop antenna (model of the left-handed square ACT-R). The simulation is performed at $f = 1.63$ GHz, where $k_0/|\beta| = 1$ (and hence loop length $n\lambda_g = n\lambda_0$) is approximately realized in the dispersion diagram at $\beta/k_0 = -1$. (a) $E_\theta^{LH,n}$, where $n = 1$ and 2. (b) $E_\phi^{LH,n}$, where $n = 1$ and 2.

square *metaloop* antenna, shown in Fig. 19, which is composed of $C$-type metaatoms. The parameters used for the simulation are the same as those shown in Table 1. Note that the conducting ground plane supporting the dielectric substrate at $z = -B$ (see Fig. 14) is removed using image theory.

Fig. 20 shows the simulated phase of the radiation field from the square metaloop antenna, where a negative $\beta$ is realized at a frequency of 1.63 GHz, where $k_0/|\beta| = 1$

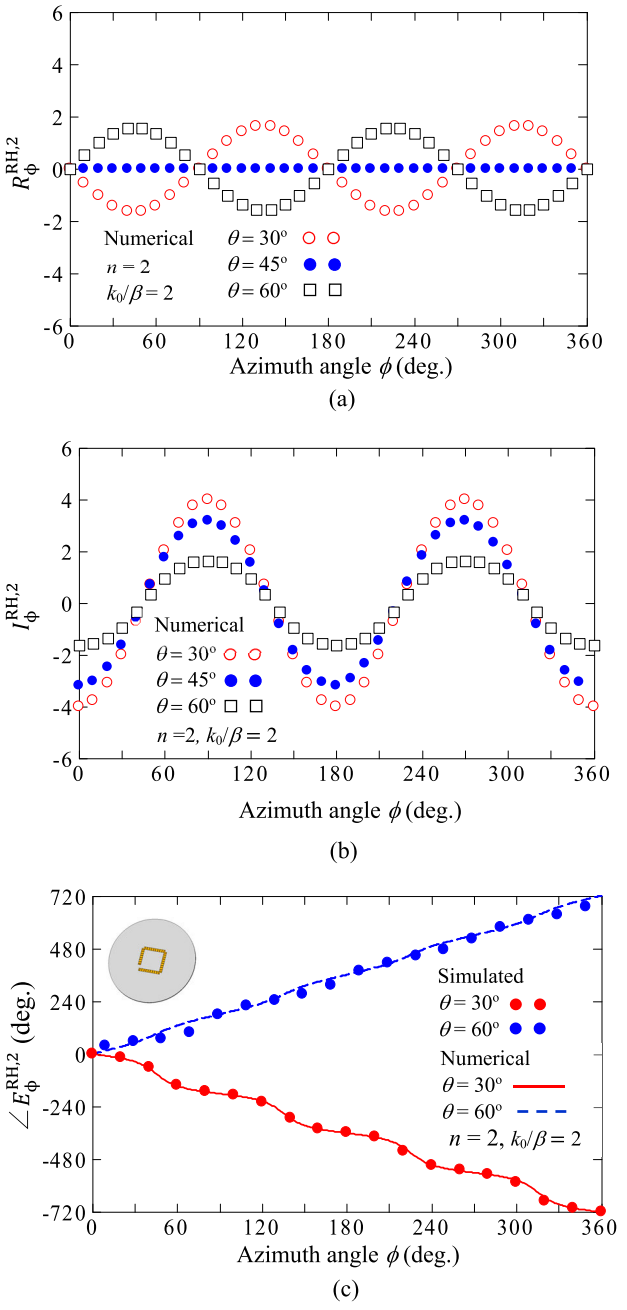


**FIGURE 21.** The $\phi$-component of the radiation field from the right-handed square ACT-R for the square metaloop antenna with $n = 2$. The simulation is performed using $f = 2.32$ GHz, where $k_0/\beta = 2$ (and hence loop length $n\lambda_g = 2n\lambda_0$) is approximately realized in the dispersion diagram at $\beta/k_0$ $[=(k_0/\beta)^{-1}] = 0.5$. (a) $R_\phi^{RH,2}$. (b) $I_\phi^{RH,2}$. (c) Standardized phase $\angle E_\phi^{RH,2}$.

(and hence loop length $n\lambda_g = n\lambda_0$) is approximately realized in the dispersion diagram of Fig. 15 at $\beta/k_0$ $[=(k_0/\beta)^{-1}] = -1$. The simulation results reveal progressive phase changes of 360° for $n = 1$ and 720° for $n = 2$, which agree with the numerical results.

## VII. SINGULAR BEHAVIOR IN THE SQUARE ACTIVE REGION OF TWO GUIDED WAVELENGTHS

The phase of the radiation field from the square ACT-R for $n = 2$ in section IV is simulated under the condition that $k_0/\beta$ is $\pm 1$ (and hence, $k_0/|\beta| = |\beta|/k_0 = 1$).

When $k_0/|\beta|$ is denoted as $h_{pcr}$, the length of ACT-R becomes $n\lambda_g = nh_{pcr}\lambda_0$; for instance, when $k_0/|\beta| = 2$, the length of ACT-R is larger than $2\lambda_0$, and it is $4\lambda_0$. This means that an antenna has a large area and causes singular behavior in the PhasProg. The large area is not desirable from a practical viewpoint of realizing a small antenna structure.

Fig. 21 shows one example where $n = 2$ and $k_0/\beta = 2$. In agreement with the general trend for positive $\beta$, a regressive PhasProg is obtained at $\theta = 30°$; however, a regressive PhasProg is not obtained at $\theta = 60°$, despite $\beta$ being positive, and a progressive PhasProg appears, as shown in Fig. 21(c). This happens before and after a depression angle of $\theta = \theta_S = \sin^{-1}(\sqrt{2}\beta/k_0) = 45°$, which is derived from $(2 - \tilde{k}^2) = 0$ in Eq. (82). Note that $k_0/\beta = 2$ (and hence $\beta/k_0 = 0.5$) is approximately realized at a frequency of 2.32 GHz in the dispersion diagram of Fig. 15.

## VIII. CONCLUSION

The radiation field from circular and square ACT-Rs is formulated, taking into account the sign of the propagation phase constant, $\beta$, of the current flowing on the ACT-R. Based on this formulation, the phase progression, PhasProg, of the radiation field after one rotation around the ACT-R axis (z-axis) is clarified.

The phase of the radiation field from the circular right-handed ACT-R of length $n\lambda_g$ ($n = 1, 2$) changes by $360n$ degrees after one rotation around the z-axis; this is obtained at *any* depression angle $\theta$. The same holds true for the circular left-handed ACT-R of length $n\lambda_g$ ($n = 1, 2$). The right-handed ACT-R has a regressive PhasProg and the left-handed ACT-R has a progressive PhasProg. Both PhasProgs for any depression angle $\theta$ form a *perfectly straight line* with respect to azimuth angle $\phi$.

Such a perfectly straight line is not found with a *square* ACT-R of length $n\lambda_g$ ($n = 1, 2$); the PhasProg forms a *quasi-straight line*, although the same change of $360n$ degrees ($n = 1, 2$) is produced, as with the circular ACT-R. Generally, the square ACT-R has a regressive PhasProg for $\beta > 0$ and a progressive PhasProg for $\beta < 0$, as long as $\theta$ is not equal to the singular angle of $\theta_S$. An investigation finds that, for the square ACT-R of length $2\lambda_g$, $\theta_S$ is likely to exist for both positive $\beta$ and negative $\beta$. As an example where $k_0/|\beta| = 2$ ($|\beta|/k_0 = 0.5$), it is revealed that a change from a regressive (progressive) PhasProg into a progressive (regressive) PhasProg in $E_\phi$ occurs when $\theta$ exceeds singular angle $\theta_S$.

The abovementioned findings are confirmed using simulated results, where natural loop and metaloop antennas are used as models for the ACT-R for $\beta > 0$ and $\beta < 0$,

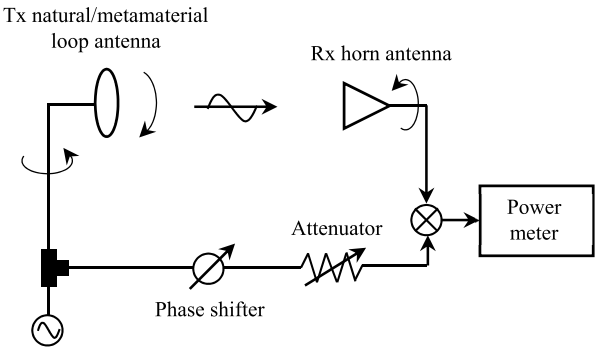


**FIGURE 22. Schematic experimental set up for measurement of the radiation phase.**

respectively. The simulated results are in good agreement with the numerical/formulated results.

Note that the concept presented in this paper is applied to a tilted beam-forming, which is realized by using summation of radiation fields generated from both $1\lambda_g$ and $2\lambda_g$ ACT-Rs. Also, note that the proposed concept could be verified by measurement. As shown in schematic figure Fig. 22 (Appendix B), the radiation field from a transmitting loop antenna (natural loop antenna for $\beta > 0$ and metamaterial loop antenna for $\beta < 0$) is sent to a power meter to mix it and make a null power by a phase- and amplitude-adjustable reference signal (field). A change in the phase of the reference signal can provide the phase of the radiation field.

## APPENDIX A

We express the $i$-component ($i = \theta, \phi$) of the radiation field generated by the current on the upper line located at z = 0 as $E_i(\theta, \phi) \equiv |E_i(\theta, \phi)|e^{j\Phi_{Ui}(\theta,\phi)}$, where $E_i(\theta, \phi)$ is a complex number and $\Phi_{Ui}(\theta, \phi)$ is its argument (phase). Then, the radiation field generated by the current on the lower line at z = $-2B$ (image line) is expressed as $-E_i(\theta, \phi)e^{-jk_0(2B)\cos\theta}$. The $i$-component of the total radiation field generated by these two currents is given as

$$E_{Ti}(\theta, \phi) = |1 - e^{-jk_0(2B)\cos\theta}| \cdot |E_i(\theta, \phi)| \cdot e^{j\Phi_{Ui}(\theta,\phi)} \cdot e^{j\Phi_{Li}(\theta)} \quad (91)$$

where

$$\Phi_{Li}(\theta) = \tan^{-1} \frac{\sin(2Bk_0\cos\theta)}{1 - \cos(2Bk_0\cos\theta)} \quad (92)$$

Therefore, the phase of the total radiation field is

$$\angle E_{Ti}(\theta, \phi) = \Phi_{Ui}(\theta, \phi) + \Phi_{Li}(\theta) \quad (93)$$

Thus, the standardized phase is

$$[\Phi_{Ui}(\theta, \phi) + \Phi_{Li}(\theta)] - [\Phi_{Ui}(\theta, \phi = 0^\circ) + \Phi_{Li}(\theta)] = \Phi_{Ui}(\theta, \phi) - \Phi_{Ui}(\theta, \phi = 0^\circ) \quad (94)$$

It follows that the standardized phase for the $i$-component due to the upper and lower currents is the same as that due to the upper current.

## APPENDIX B

See Figure 22.

## ACKNOWLEDGMENT

The authors thank V. Shkawrytko for his assistance in the preparation of this manuscript.

## REFERENCES

[1] I. J. Bahl and P. Bhartia, *Microstrip Antennas*. Norwood, MA, USA: Artech House, 1980.
[2] J. R. James and P. S. Hall, and C. Wood, *Microstrip Antenna*. Stevenage, U.K.: Peter Peregrinus, 1981.
[3] J. Kaiser, "The archimedean two-wire spiral antenna," *IRE Trans. Antennas Propag.*, vol. 8, no. 3, pp. 312–323, May 1960.
[4] V. H. Rumsey, *Frequency Independent Antennas*. New York, NY, USA: Academic, 1966.
[5] T. P. Cencich and D. S. Filipovic, "Spiral antennas," in *Encyclopedia of RF and Microwave Engineering*, vol. 5, K. Chang, Ed. Hoboken, NJ, USA: Wiley, 2005, pp. 4853–4869.
[6] H. Nakano, K. Nogami, S. Arai, H. Mimaki, and J. Yamauchi, "A spiral antenna backed by a conducting plane reflector," *IEEE Trans. Antennas Propag.*, vol. AP-34, no. 6, pp. 791–796, Jun. 1986.
[7] H. Nakano, J. Miyake, M. Oyama, and J. Yamauchi, "Metamaterial spiral antenna," *IEEE Antennas Wireless Propag. Lett.*, vol. 10, pp. 1555–1558, 2011.
[8] G. Li, G. Gao, W. Liu, and Z. Tian, "Tunable and flexible liquid spiral antennas," *Electron. Lett.*, vol. 53, no. 10, pp. 648–650, May 2017.
[9] H. Nakano, S. Okuzawa, K. Ohishi, H. Mimaki, and J. Yamauchi, "A curl antenna," *IEEE Trans. Antennas Propag.*, vol. 41, no. 11, pp. 1570–1575, Nov. 1993.
[10] S. M. O'Kane and V. F. Fusco, "Circularly polarized curl antenna lens with manual tilt properties," *IEEE Trans. Antennas Propag.*, vol. 57, no. 12, pp. 3984–3987, Dec. 2009.
[11] H. Nakano, J. Miyake, T. Sakurada, and J. Yamauchi, "Dual-band counter circularly polarized radiation from a single-arm metamaterial-based spiral antenna," *IEEE Trans. Antennas Propag.*, vol. 61, no. 6, pp. 2938–2947, Jun. 2013.
[12] K. Hirose, T. Shibasaki, and H. Nakano, "Fundamental study on novel loop-line antennas radiating a circularly polarized wave," *IEEE Antennas Wireless Propag. Lett.*, vol. 11, pp. 476–479, 2012.
[13] H. Nakano, "A numerical approach to line antennas printed on dielectric materials," *Comput. Phys. Commun.*, vol. 68, nos. 1–3, pp. 441–450, Nov. 1991.
[14] P. J. Massey, P. Fellows, D. Mirshekar-Syahkal, A. Pal, and A. Mehta, "Loop antennas," in *Handbook Antenna Technol.*, vol. 2, Z. Chen, D. Liu, H. Nakano, X. Qing, and T. Zwick, Eds. Singapore: Springer, 2016, pp. 723–786.
[15] L. W. Rispin and D. C. Chang, "Wire and loop antennas," in *Antenna Handbook*, Y. T. Lo and S. W. Lee, Eds. New York, NY, USA: Van Nostrand, 1988.
[16] C. Deng, Y. Li, Z. Zhang, and Z. Feng, "A hemispherical 3-D null steering antenna for circular polarization," *IEEE Antennas Wireless Propag. Lett.*, vol. 14, pp. 803–806, 2015.
[17] H. Nakano, T. Abe, T. Kawano, A. Mehta, and J. Yamauchi, "Azimuth angle estimation for a reduced radiation region formed by a metaspiral antenna," *IEEE Access*, vol. 7, pp. 78289–78297, Jun. 2019.
[18] Darmstadt, Germany, Microwave Studio. *CST Computer Simulation Technology GmbH*. Accessed: Dec. 2020. [Online]. Available: http://www.cst.com
[19] C. Caloz and T. Itoh, *Electromagnetic Metamaterials*. Hoboken, NJ, USA: Wiley, 2006.
[20] H. Nakano, K. Sakata, and J. Yamauchi, "Linearly and circularly polarized radiation from metaline antennas," in *Proc. Int. Workshop Antenna Technol. (iWAT)*, Cocoa Beach, FL, USA, Feb. 2016, pp. 142–143.

**HISAMATSU NAKANO** (Life Fellow, IEEE) has been with Hosei University, since 1973, where he is currently a Professor Emeritus and a Special-appointment Researcher with the Electromagnetic Wave Engineering Research Institute attached to the graduate school. He has held positions as a Visiting Associate Professor at Syracuse University, from March to September 1981, a Visiting Professor at the University of Manitoba, from March to September 1986, the University of California at Los Angeles, from September 1986 to March 1987, and Swansea University, U.K., from July–September 2016 to 2019. He has published over 330 articles in peer-reviewed journals and 11 books/book chapters, including *Low-profile Natural and Metamaterial Antennas* (IEEE Press, Wiley, 2016). His significant contributions are the development of five integral equations for line antennas in free space and printed on a dielectric substrate, the invention of an L-shaped wire/strip antenna feeding method, and the realization of numerous wideband antennas, including curl, metaspiral, metahelical, and body-of-revolution antennas. His other accomplishments include design of antennas for GPS, personal handy phones, space radio, electronic toll collection, RFID, UWB, and radar. He has been awarded 78 patents, including *A Curl Antenna Element and Its Array* (Japan). His research interests include numerical methods for low- and high-frequency antennas and optical waveguides. He served as a member for the IEEE APS Administrative Committee, from 2000 to 2002, and a Region 10 Representative, from 2001 to 2010. He received the H. A. Wheeler Award in 1994, the Chen-To Tai Distinguished Educator Award in 2006, and the Distinguished Achievement Award in 2016 from the IEEE Antennas and Propagation Society. He was a recipient of The Prize for Science and Technology from Japan's Minister of Education, Culture, Sports, Science and Technology, in 2010. He was selected as a recipient of the Antenna Award of the European Association on Antennas and Propagation (EurAAP), in 2020. He is also an Associate Editor for several scientific journals and magazines, such as *Electromagnetics* and the *IEEE Antennas and Propagation Magazine*.

**TOMOKI ABE** (Member, IEEE) was born in Miyagi, Japan, in August 12, 1994. He received the B.E. and M.E. degrees in electronics and electrical engineering from Hosei University, Tokyo, Japan, in 2017 and 2019, respectively. He is a member of the Institute of Electronics, Information and Communication Engineers of Japan.

**JUNJI YAMAUCHI** (Life Fellow, IEEE) was born in Nagoya, Japan, in August 23, 1953. He received the B.E., M.E., and Dr.E. degrees from Hosei University, Tokyo, Japan, in 1976, 1978, and 1982, respectively. From 1984 to 1988, he was a Lecturer with the Department of Electrical Engineering, Tokyo Metropolitan Technical College. Since 1988, he has been a member of the faculty of Hosei University, where he is currently a Professor with the Department of Electrical and Electronic Engineering. His research interests include optical waveguides, polarization converters, and circularly polarized antennas. He is the author of *Propagating Beam Analysis of Optical Waveguides* (Research Studies Press, 2003). He is a member of the Optical Society of America and the Institute of Electronics, Information and Communication Engineers of Japan.